

Experimental investigation on divertor tungsten sputtering with neon seeding in ELMy H-mode plasma in EAST tokamak

Dawei Ye(叶大为), Fang Ding(丁芳), Kedong Li(李克栋), Zhenhua Hu(胡振华), Ling Zhang(张凌), Xiahua Chen(陈夏华), Qin Zhang(张青), Pingan Zhao(赵平安), Tao He(贺涛), Lingyi Meng(孟令义), Kaixuan Ye(叶凯萱), Fubin Zhong(钟富彬), Yanmin Duan(段艳敏), Rui Ding(丁锐), Liang Wang(王亮), Guoshen Xu(徐国盛), Guangnan Luo(罗广南), and EAST team

Citation: Chin. Phys. B, 2022, 31 (**6**): 065201. DOI: 10.1088/1674-1056/ac4f58
Journal homepage: http://cpb.iphy.ac.cn; http://iopscience.iop.org/cpb

What follows is a list of articles you may be interested in

Observation of trapped and passing runaway electrons by infrared camera in the EAST tokamak

Yong-Kuan Zhang(张永宽), Rui-Jie Zhou(周瑞杰), Li-Qun Hu(胡立群), Mei-Wen Chen(陈美文), Yan Chao(晁燕), Jia-Yuan Zhang(张家源), and Pan Li(李磐)
Chin. Phys. B, 2021, 30 (**5**): 055206. DOI: 10.1088/1674-1056/abd758

Analysis of asymmetry of the D_α emission spectra under the Zeeman effect in boundary region for D-D experiment on EAST tokamak

Wei Gao(高伟), Juan Huang(黄娟), Jianxun Su(宿建勋), Jing Fu(付静), Yingjie Chen(陈颖杰), Wei Gao(高伟), Zhenwei Wu(吴振伟), and EAST Team
Chin. Phys. B, 2021, 30 (**2**): 025201. DOI: 10.1088/1674-1056/abc162

Measurement of molybdenum ion density for L-mode and H-mode plasma discharges in the EAST tokamak

Yongcai Shen(沈永才), Hongming Zhang(张洪明), Bo Lyu(吕波), Yingying Li(李颖颖), Jia Fu(符佳), Fudi Wang(王福地), Qing Zang(臧庆), Baonian Wan(万宝年), Pan Pan(潘盼), Minyou Ye(叶民友)
Chin. Phys. B, 2020, 29 (**6**): 065206. DOI: 10.1088/1674-1056/ab8456

Observation of deuterium molecule emission spectra under an active feedback control of H-mod plasma divertor detachment experiment on the EAST tokamak

Wei Gao(高伟), Juan Huang(黄娟), Jichan Xu(许吉禅), Liang Wang(王亮), Jing Zhang(张静), Jianxun Su(宿建勋), Yingjie Chen(陈颖杰), Wei Gao(高伟), Zhenwei Wu(吴振伟), EAST Team
Chin. Phys. B, 2019, 28 (**12**): 125202. DOI: 10.1088/1674-1056/ab54b2

Experimental investigation on divertor tungsten sputtering with neon seeding in ELMy H-mode plasma in EAST tokamak

Dawei Ye(叶大为)[1,2], Fang Ding(丁芳)[1,†], Kedong Li(李克栋)[1,2], Zhenhua Hu(胡振华)[1], Ling Zhang(张凌)[1], Xiahua Chen(陈夏华)[1,2], Qing Zhang(张青)[1,2], Pingan Zhao(赵平安)[1,2], Tao He(贺涛)[1,2], Lingyi Meng(孟令义)[1,2], Kaixuan Ye(叶凯萱)[1], Fubin Zhong(钟富彬)[1], Yanmin Duan(段艳敏)[1], Rui Ding(丁锐)[1], Liang Wang(王亮)[1], Guosheng Xu(徐国盛)[1], Guangnan Luo(罗广南)[1,2], and EAST team

[1] *Institute of Plasma Physics, HFIPS, Chinese Academy of Sciences (CAS), Hefei* 230031, *China*
[2] *University of Science and Technology of China, Hefei* 230026, *China*

(Received 22 December 2021; revised manuscript received 22 January 2022; accepted manuscript online 27 January 2022)

Neon (Ne) seeding is used to cool the edge plasma by radiation to protect the divertor tungsten (W) target in the Experimental Advanced Superconducting Tokamak (EAST). The W sputtering in the outer divertor target with Ne seeding is assessed by the divertor visible spectroscopy system. It is observed that the W sputtering flux initially increases with Ne concentration in the divertor despite the decreasing plasma temperature. After reaching a maximum around 25 eV, the W sputtering rate starts to decrease, presenting a suppression effect. The effect on the divertor W sputtering flux and yield due to the competition between the increase of the Ne concentration and the decrease of the plasma temperature is discussed. The results show that enough Ne seeding is essential to effectively reduce the electron temperature and thus to suppress W sputtering. Moreover, ELM suppression is observed when Ne and W impurities enter the core plasma, which could be correlated to the enhanced turbulence transport in the pedestal.

Keywords: neon seeding, tungsten sputtering, ELM suppression, EAST tokamak

PACS: 52.25.Vy, 52.40.Hf, 52.30.Cv, 52.55.Fa **DOI:** 10.1088/1674-1056/ac4f58

1. Introduction

Tungsten (W) is foreseen as the most promising plasma-facing material (PFM) for the divertor in the ITER in terms of its high melting temperature, low sputtering yields and low deuterium retention rate.[1] With the increase of heating power in future fusion devices, extremely high power fluxes onto the divertor can cause significant erosion of the divertor material. Due to the absence of the intrinsic impurity radiation in full metal wall devices, extrinsic impurity seeding is considered as an indispensable way to reduce the energy deposited on the target. Simulations have shown that both neon (Ne) and nitrogen (N_2) seeding can be used to dissipate significant amounts of power and to reduce the heat load on the divertor to an acceptable level (5 MW/m^2–10 MW/m^2) in ITER.[2] Although N_2 shows beneficial results in confinement enhancement and radiation increase in the edge plasma, the formation of partially tritiated ammonia affects the machine duty cycle in ITER deuterium–tritium plasma.[3] Therefore, Ne seems to be a better radiator in future fusion devices. However, as the W sputtering yield depends strongly on the incident particle species and their energies, Ne has a higher W sputtering yield than that of deuterium (D) or tritium (T) at the same incidence energy.[1] The existing simulation results reveal that the insufficient seeded Ne impurity could reduce the heat flux to the target, but the erosion of the W target can be obviously enhanced.[4] When the detached condition is achieved with sufficient Ne seeding, the W target erosion is obviously suppressed. In this work, the behaviors of W sputtering with Ne seeding in the divertor are experimentally observed and analyzed on EAST. The experiments reveal that the evolution of both the W sputtering rate and yield at the divertor target can be the competing results between two seeding effects, increasing divertor Ne impurity content and decreasing electron temperature, which is consistent with the simulation results.[4] In addition, ELM suppression has been observed in this Ne seeding experiment. Due to the W sputtering by seeded Ne impurities, both the W and Ne impurities in the core plasma significantly increase after Ne seeding in the upper divertor. The influence of Ne and W impurities on ELM behavior is discussed.

The rest of this paper is organized as follows: The experimental setup and method are introduced in Section 2. The effects of Ne seeding on divertor W sputtering are given in Section 3. The influence of impurity on the ELM is discussed in Section 4. Summary is presented in Section 5.

2. Experimental setup and method

EAST is an experimental superconducting tokamak device with a D-shaped poloidal cross-section and flexible di-

†Corresponding author. E-mail: fding@ipp.ac.cn
© 2022 Chinese Physical Society and IOP Publishing Ltd

vertor configurations, aiming at long-pulse high-performance H-mode operations.[5] The top W divertor with actively cooled ITER-like monoblock structure was installed in 2014[6] while the bottom W divertor was installed in 2021.[7] This work was carried out with the upper W divertor and lower previous graphite divertor as shown in Fig. 1(a). Meanwhile, the first wall in the main chamber is covered by molybdenum and graphite tiles.[7] EAST is equipped with a set of gas puff inlets distributed at the outer target, inner target, and dome of both top and bottom divertors. Only the inlet at the upper inner (UI) target was used for impurity seeding in this work as shown in Fig. 1(b). The impurity seeding rate can be adjusted by changing the pulse voltage, duty, and frequency applied on the piezoelectric valve.

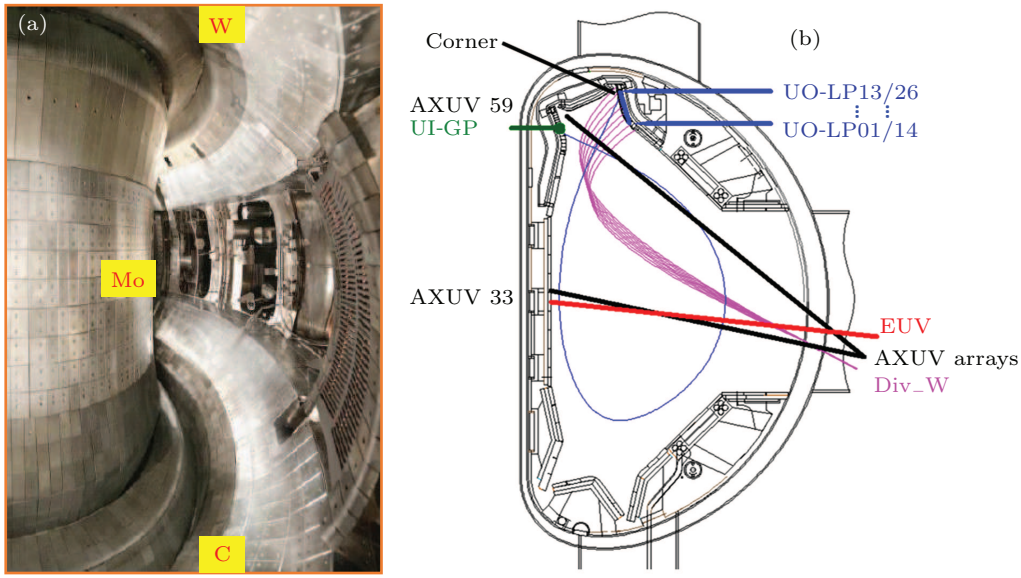


Fig. 1. (a) View into the EAST vacuum chamber and (b) geometry of viewing chords for the diagnostics used in this paper. Div-W (magenta): multichannel visible spectroscopy viewing the upper outer (UO) tungsten divertor; EUV (orange): extreme ultraviolet spectrometer; AXUV arrays (black): absolute extreme ultraviolet photodiode arrays with two bold lines indicating the 33th and 59th channels passing through the core and upper divertor region, respectively; UO-LP (blue): divertor Langmuir probes at the UO target, UO-LP01 to UO-LP13 at port D and UO-LP14 to UO-LP26 at port O; UI-GP (green): gas puff inlet at the upper inner (UI) target. A typical separatrix of main plasma is also shown with the blue line.

The multichannel visible spectroscopy system (Div-W) located in the equatorial port H[8] is used to monitor impurity line emissions especially the W I line at 400.88 nm in the upper divertor region. A schematic diagram of the lines of sight of the Div-W system is shown in Fig. 1(b). The spatial resolution along the divertor targets is 13 mm and the temporal resolution is 5 ms in this work. Figure 2 shows a typical spectrum in the wavelength range of 396.2 nm to 427. nm with Ne seeding in the UI divertor. The line intensity of W I at 400.88 nm is used to quantify the W atom influx $\Gamma_{\rm W}$ by applying the inverse photon efficiency.[9] The W atom influx can be written as a function of the line intensity:[10]

$$\Gamma_{\rm W} = 4\pi \frac{S}{XB}(T_{\rm e}) I_{\rm WI}, \tag{1}$$

where S/XB is the inverse photon efficiency, and $I_{\rm WI}$ is the W I line emission intensity. Here, S, X, and B denote the ionization and excitation rate coefficients, and the branching ratio for emission, respectively. We estimated the value of S/XB by using the following formula to incorporate its dependence on the plasma temperature $T_{\rm e}$ (in unit eV):[11]

$$\frac{S}{XB}(T_{\rm e}) = 53.7\left(1 - 1.04\exp\left(\frac{T_{\rm e}}{22.1}\right)\right). \tag{2}$$

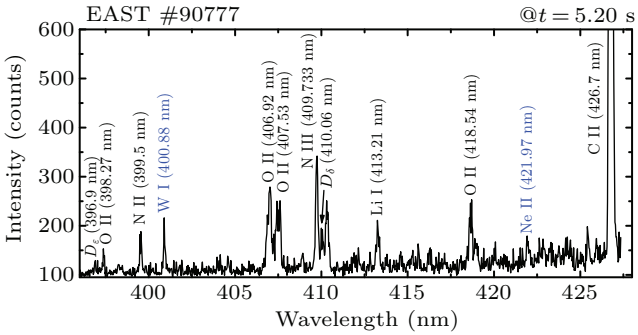


Fig. 2. A typical spectrum in wavelength ranges of 396.2 nm–427.6 nm obtained by the Div-W system in the USN H-mode plasma with Ne seeding.

In addition to the W I line at 400.88 nm, some low Z impurity lines as well as neutral deuterium atom lines are also observed by the Div-W system as shown in Fig. 2, including O II (398.27 nm, 406.92 nm, 407.53 nm, 418.54 nm), N II (399.5 nm), N III (409.733 nm), Ne II (421.97 nm), Li I (413.21 nm), C II (426.7 nm), D_δ (410.06 nm), D_ε (396.9 nm) *etc*. These emission lines are in good agreement with the NIST atomic spectra database. The high strength of the C II line in this spectral range can be attributed to the erosion of graphite plasma-facing components (PFCs) in the lower divertor and the guard limiter of antennae. Due to the lithium coating, the Li I line can be detected and used to evaluate wall coating conditions.[12] Line emissions from low-ionized oxygen and

nitrogen ions may be due to the residual air absorbed in the PFCs and structural materials. The characteristic spectral line Ne II can be used as an indicator of Ne ion flux to the divertor target.[11]

Figure 1(b) illustrates the relevant diagnostics used in this work. In addition to the Div-W system, the absolute extreme ultraviolet (AXUV) photodiode arrays provide measurements of the radiated power in EAST plasma with fast temporal response (4 μs) and flat spectral sensitivity in the range from ultraviolet to x-ray.[13] Among 64 channels of the AXUV system, the 33th channel passes through the plasma core and the 59th channel views the upper divertor through the X-point region. The electron temperature (T_{et}) and ion saturation current (j_{sat}) at the divertor target are measured by Langmuir probes embedded in the divertor target plate with a poloidal resolution of 12 mm–18 mm.[14] The line emissions of highly ionized impurities in the plasma core including W and Ne can be detected by the fast-time-response extreme ultraviolet (EUV) spectrometer in the wavelength range of 1 nm–50 nm.[15] An unresolved transition array (W-UTA) of tungsten ions in the core plasma, consisting of ionization stages in W^{27+}–W^{45+}, is clearly observed with strong intensity in the wavelength range of 4.5 nm–7.0 nm.[16] Thus the W-UTA signal provides an approximate estimation of the content of tungsten in the core plasma. The Ne X line intensity at 1.213 nm measured by the EUV system is used to monitor the Ne impurity content in the core plasma.

3. Effect of Ne seeding on divertor W sputtering

Ne impurity is normally seeded into the EAST W divertor to enhance the plasma radiation in order to achieve plasma detachment.[17] Figure 3 shows the time evolutions of the major plasma parameters in the USN H-mode discharge #90777 with Ne mixed gas seeding (volume ratio, Ne:D_2 = 1 : 1). This discharge was operated in the favorable toroidal magnetic field direction with $B_t = 2.5$ T, plasma current $I_p = 400$ kA, power injection of lower hybrid wave $P_{LHW} = 2.5$ MW (Fig. 3(a)), power injection of neutral beam injection $P_{NBI} = 3.0$ MW (Fig. 3(a)) and plasma stored energy $W_{MHD} = 150$ kJ. Figure 3(a) shows that the voltage pulse of Ne seeding in the upper divertor starts at 4 s and lasts for about 500 ms. Most of the plasma parameters start to respond after a delay of about 400 ms. The time delay should be due to gas flowing in the pipe between the gas valve outside the machine and the gas inlet in the divertor. Afterwards the central line-averaged electron density n_{el} increases from 3.0×10^{19} m^{-3} to 3.5×10^{19} m^{-3} (Fig. 3(b)) and the peak ion saturation current density (j_{sat}) at the upper outer divertor target increases slightly from 1.5 A/cm^2 to 2 A/cm^2 (Fig. 3(e)). The Ne II line emission in the divertor gradually increases until twice the value before seeding (Fig. 3(c)).

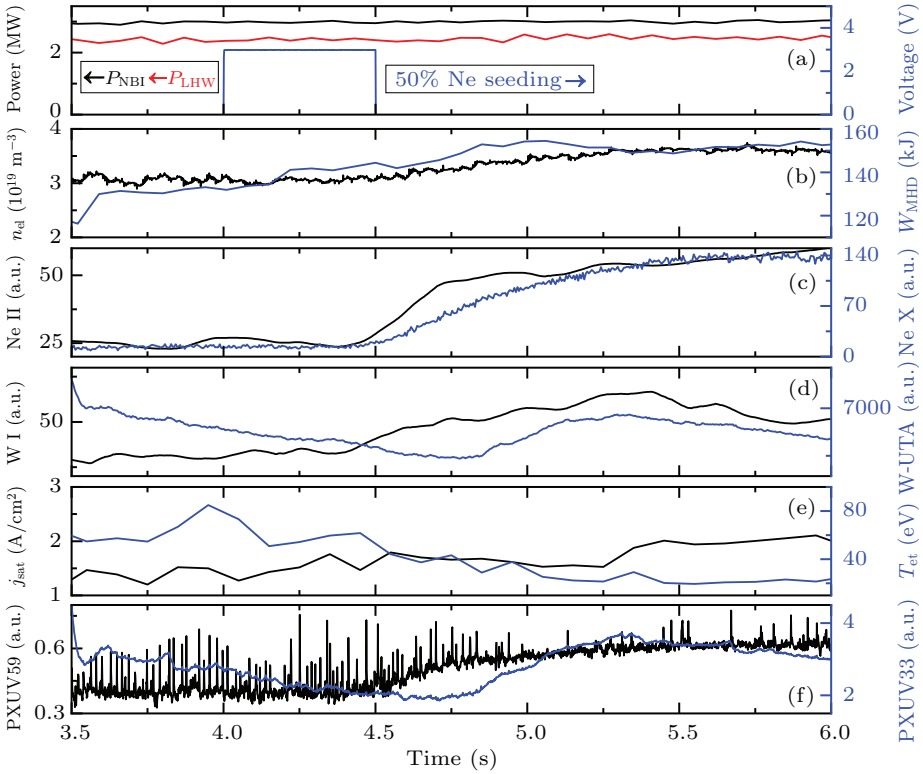


Fig. 3. Time evolutions of the experimental parameters in discharge #90777 with Ne seeding. (a) Power source of NBI (black) and LHW (red) heating, and the voltage signal of the piezo valve for Ne seeding (blue); (b) the line-averaged electron density at the mid-plane n_{el} (black) and plasma stored energy W_{MHD} (blue); (c) Ne II line (black) emission measured by Div-W and Ne X line (blue) emission measured by EUV; (d) W I line emission measured by Div-W (black) and W-UTA measured by EUV (blue); (e) ion saturation current j_{sat} (black) and peak electron temperature T_{et} (blue) at the UO target measured by divertor Langmuir probes; (f) AXUV 59th channel (black) measuring radiation across the upper divertor and AXUV 33th channel (blue) measuring radiation across the plasma core. The unit a.u. is short for arb. units.

Figure 3(f) shows the upper divertor radiation measured by the 59th channel of AXUV across the upper divertor has a similar trend as the Ne II line emission, indicating that Ne seeding could enhance the plasma radiation in the divertor. This could explain the decrease of T_{et} at the UO target from $\sim$ 50 eV to 20 eV due to the radiation cooling effect as shown in Fig. 3(e). Despite the reduction of incident ion energy (proportional to T_{et}), the W I line emission presents a rising trend until 5.3 s and then starts to drop (Fig. 3(d)).

Figure 4 shows the distributions of W I line emission and T_{et} along the upper outer (UO) target. The x axis represents the distance along the UO target to the corner between the outer target and the dome as indicated in Fig. 1(b). The profile of W I line emission along the target is similar to that of T_{et}, indicating the strong dependence of the W sputtering rate on the incident ion energy in the spatial distribution. However, it is also seen that the W I line emissions around the peak keep increasing with time before reaching a maximum around 5.3 s, which is opposite to the temporal evolution of the corresponding T_{et}.

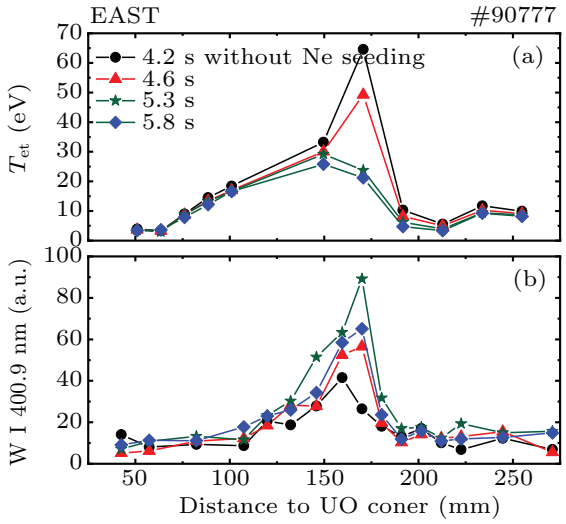


Fig. 4. Profiles at 4 different times of (a) W I line emission at 400.9 nm and (b) electron temperature T_{et} along the UO divertor target in discharge #90777 with Ne seeding.

To further understand the W sputtering behavior with Ne seeding, both the W atom flux (Γ_W) and effective W sputtering yield ($Y_{W,phy} = \Gamma_W / j_{sat}$) are quantified based on the method as described in Section 2. Figures 5(b) and 5(c) plot the peak Γ_W and $Y_{W,phy}$ against the peak T_{et} and the Ne II line emission, respectively. Moreover, the dependences of T_{et} and j_{sat} on the Ne II line emission are also illustrated in Fig. 5(a). It can be seen in Fig. 5(a) that the T_{et} drops from 50 eV to 18 eV and the j_{sat} rises slightly from 1.5 A/cm^2 to 2 A/cm^2 with the increase of the Ne II line emission. Especially when the relative Ne II line intensity exceeds 45, a rapid rise appears for j_{sat} and then T_{et} decreases to below 20 eV, which may indicate that the divertor plasma goes into a high recycling regime. These reveal that Ne seeding could change divertor plasma status and effectively reduce T_{et} at the divertor target, thus causing a decrease of ion impact energy on W surface. However, the sputtered W atom flux does not present an immediate drop with the decrease of T_{et} as shown in Fig. 5(b).

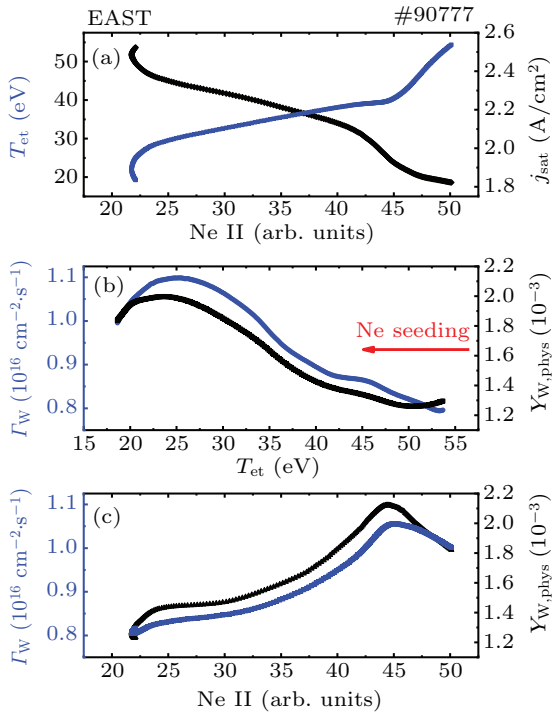


Fig. 5. Effects of Ne seeding on the W sputtering at the UO divertor target. (a) Peak T_{et} and j_{sat} at the UO target as a function of Ne II line emission intensity; (b) peak W atom flux Γ_W and effective tungsten sputtering yield $Y_{W,phys} (= \Gamma_W / j_{sat})$ as a function of T_{et}; (c) peak Γ_W and $Y_{W,phys}$ as a function of Ne II line emission intensity.

On the contrary, the W atom flux Γ_W initially increases with the decrease of T_{et} until 25 eV. Then after a rollover, Γ_W starts to decrease with T_{et}. The same trend is also observed for effective W sputtering yield $Y_{W,phy}$, implying the dominant role of $Y_{W,phy}$ in the evolution of Γ_W. Calculations by TRIM[18] in the binary-collision approximation predict that both the impact energy and the mass of incident particle have strong influences on the sputtering yield. The Monte Carlo simulation by Ou *et al.* also shows similar dependence of the W physical sputtering yield on the bombardment energy and different impurity ions.[19] Thus, it is considered that the Ne seeding decreases the divertor plasma temperature to reduce the impact energy of the incident particles on the one hand, but increases the Ne impurity concentration in the divertor plasma on the other hand. The dependence of W sputtering on T_{et}, as shown in Fig. 5(b), should result from the competition between the above two effects. The W sputtering increases gradually upon Ne seeding and the T_{et} decreases from 50 eV to 25 eV, where the Ne induced sputtering effect dominates. The W sputtering flux is observed to reach a maximum at 25 eV, nearly 50% increase relative to that before Ne seeding. The Ne seeding starts to have a net beneficial effect on the suppression of W sputtering when T_{et} drops below 25 eV, where the cooling effect of Ne seeding dominates. A rollover for both sputtering atom flux (Γ_W) and yield ($Y_{W,phy}$) similar to that in Fig. 5(b) is

also observed in Fig. 5(c) when the relative Ne II line intensity exceeds 45 and the divertor plasma goes into a high recycling regime. These imply that the lower W sputtering rate due to the lower T_{et} in the high recycling regime could make compensation for the enhanced W sputtering by Ne impurity and the decreasing W redeposition rate, thus benefiting the control of core tungsten concentration as shown in Fig. 3(d) that is to be discussed in the next section. This experimental observation is consistent with the simulation results in Refs. [20,21]. Due to the increase of particle flux onto the target with Ne seeding as shown in Fig. 5(a), the W sputtering rate Γ_W has a faster rise before the rollover, but a slower drop after the rollover than the W sputtering yield $Y_{W,phy}$. Therefore, small amount of Ne seeding enhances the W sputtering. Only when enough Ne particles are injected into the divertor plasma to reduce the plasma temperature sufficiently, can the W sputtering be effectively suppressed.

4. Influence of impurity on the ELM

Divertor impurities can partly transport into the core plasma due to the ion temperature gradient force, *i.e.* divertor impurity leakage.[22] It can be seen in Fig. 3 that both the seeded Ne impurity and the sputtered W impurity in the UO divertor have strong influences on the main plasma. Figure 3(c) shows that the Ne X line emission at 1.213 nm starts to rise at 4.5 s after an $\sim$ 100 ms delay relative to the Ne II line emission in the divertor, indicating the penetration of Ne impurities seeded from the divertor into the core plasma. However, no obvious rise appears in the core XUV radiation signal (AXUV33 in Fig. 3(f)) at this time, although the divertor radiation channel AXUV59 presents a corresponding rise with the Ne II line emission. This indicates that the radiation contribution from Ne impurities in the core is moderate. Comparing the W-UTA spectral signal from the core W impurities and the AXUV33 signal as demonstrated in Figs. 3(d) and 3(f), a good synchronization can be observed, indicating that the core plasma radiation is dominated by the W impurity. The rise of the W-UTA signal starting at 4.8 s should be related to inward transport of the W atoms sputtered in the divertor as discussed in Section 3. The W-UTA signal presents a good correlation with the W I signal in Fig. 3(d) since 4.8 s. The slow decrease of W-UTA intensity before 4.8 s is a recovery process after another W impurity event. In general, the plasma stored energy (W_{MHD}) presents an opposite evolution with core tungsten radiation loss as shown in Fig. 3. Moreover, the increasing density in the core should result from the injection of Ne mixture and partly contribute to the rise of plasma stored energy before 5 s, as shown in Fig. 3(b). The subsequent decrease in plasma stored energy should be related to the increasing core W impurity radiation loss. It is also noticed that ELMs are evidently suppressed since 4.8 s, coincident with the rise of the W-UTA signal.

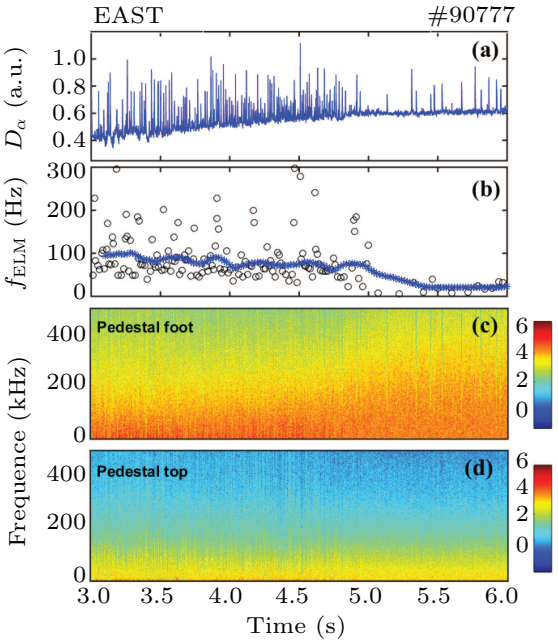


Fig. 6. Experimental results of ELM suppression during Ne seeding in #90777. (a) D_α signal in the upper divertor region; (b) ELM frequency; (c) and (d) the density fluctuation power spectra in the pedestal foot and pedestal top, respectively.

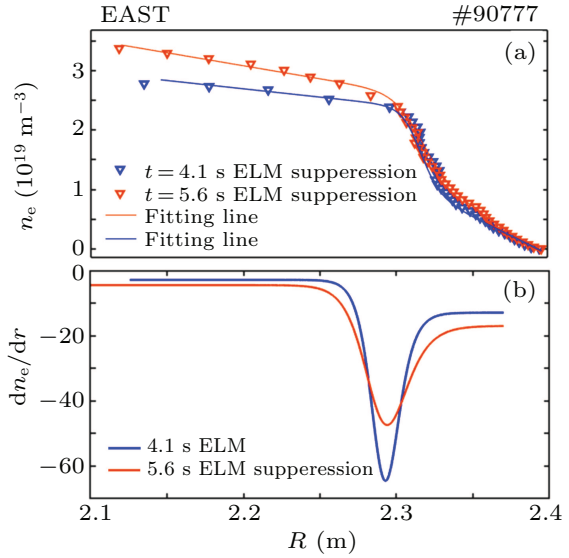


Fig. 7. (a) Density profiles reconstructed by the microwave reflectometry system at different times in the discharge #90777; (b) density gradient dn_e/dr corresponding to the curves in panel (a).

Figure 6 illustrates the temporal evolutions of the ELM frequency and the density fluctuation power spectra in the pedestal top and pedestal foot obtained by the microwave reflectometry.[23] The ELM frequency in Fig. 6(b) is calculated based on the divertor D_α signal in Fig. 6(a). The averaged ELM frequency (f_{ELM}) maintains at $\sim$ 100 Hz before 4.8 s. Most ELMs are suppressed since 4.8 s when the core W-UTA signal starts to rise. Simultaneously, figure 6(c) shows that the density fluctuation at the pedestal foot increases significantly with the rise of core plasma radiation, in which the

fluctuations with higher frequency up to 400 kHz are excited after 4.8 s. This shows that the ELM suppression could be correlated to the enhanced transport induced by turbulence in the pedestal. The impurity transport across the pedestal may play an important role, which is similar to the observations in the HL-2A tokamak.[24] Figure 7 displays two density profiles measured by the microwave reflectometry before and during the ELM supersession.[25] The density gradient in the pedestal is softened during ELM suppression compared with that before, which could be attributed to the enhanced pedestal transport. These results indicate that ELMs can be suppressed due to the changed pedestal transport by impurities.

5. Summary

The influence of Ne seeding on the tungsten sputtering from the divertor target is investigated in the EAST experiment. The sputtered W atom influx at the divertor target has been quantified by using the spectroscopic observation on W I line emission at 400.88 nm. It is found that the W sputtering rate keeps an increasing trend with Ne seeding until the electron temperature at the target drops to below 25 eV where the W sputtering reaches the maximum. The competition between the drop of plasma temperature due to the radiation cooling effect of Ne impurities and the enhancement of W sputtering yield induced by the increased Ne impurity concentration in the divertor is the main reason. Enough plasma cooling is needed to obtain a beneficial W sputtering suppression for Ne impurity seeding. Moreover, the core plasma radiation is dominated by the W impurity content in the core and strongly correlated to the W source. The ELM suppression and enhanced turbulence transport in the pedestal are observed when the impurity radiation in main plasma exceeds a threshold, demonstrating the strong influences of divertor impurities on pedestal plasma behavior.

Acknowledgements

Project supported by the National Key Research and Development Program of China (Grant Nos. 2017YFE0301300, 2017YFA0402500, and 2018YFE0303103), the National Natural Science Foundation of China (Grant Nos. 12192283 and 12022511), the Users with Excellence Project of Hefei Science Center, CAS (Grant No. 2018HSC-UE008), the CASHIPS Director's Fund (Grant No. BJPY2019B01), the JSPS-CAS Bilateral Joint Research Project (Grant No. GJHZ201984), and the Key Research Program of Frontier Sciences of CAS (Grant No. ZDBS-LY-SLH010).

References

[1] Naujoks D, Asmussen K, Bessenrodt-Weberpals M, Deschka S, Dux R, Engelhardt W, Field A R, Fussmann G, Fuchs J C and Garcia-Rosales C 1996 *Nucl. Fusion* **36** 671

[2] Sytova E, Pitts R A, Kaveeva E, Bonnin X and Reimold F 2019 *Nucl. Mater. Energy* **19** 72

[3] Drenik A, Laguardia L, McDermott R, Meisl G, Neu R, Oberkofler M, Pawelec E, Pitts R A, Potzel S, Pütterich T, Reichbauer T, Rohde V, Seibt M, De Temmerman G and Zaplotnik R 2019 *Nucl. Fusion* **59** 046010

[4] Zhao X, Sang C, Zhou Q, Zhang C, Zhang Y, Ding R, Ding F and Wang D 2020 *Plasma Phys. Control. Fusion* **62** 055015

[5] Wan Y X, HT-7 Team and HT-7U Team 2000 *Nucl. Fusion* **40** 1057

[6] Zhou Z B, Yao D M and Cao L 2014 *J. Fusion Energy* **34** 93

[7] Xu G S, Wang L, Yao D M, Jia G Z, Sang C F, Liu X J, Chen Y P, Si H, Yang Z S, Guo H Y, Du H L, Luo Z P, Li H, Zhou Z B, Cao L, Xu H C, Xu T J, Wang Z L, Zi P F, Li L, Han L, Xu J C, Liu J B, Li K D, Cao B, Yu Y W, Ding F, Ding R, Yan N, Meng L Y, Tao Y Q, Wang H Q, Zhang Y, Shao L M, Zhang X D, Zhu S Z, Wan B N and East Team 2021 *Nucl. Fusion* **61** 126070

[8] Mao H, Ding F, Luo G N, Hu Z, Chen X, Xu F, Yang Z, Chen J, Wang L, Ding R, Zhang L, Gao W, Xu J and Wu C 2017 *Rev. Sci. Instrum.* **88** 043502

[9] Behringer K, Summers H P and Denne B 1989 *Plasma Phys. Control. Fusion* **31** 2059

[10] Pospieszczyk A, Borodin D, Brezinsek S, Huber A, Kirschner A, Mertens P, Sergienko G, Schweer B, Beigman I L and Vainshtein L 2010 *J. Phys. B: At. Mol. Opt. Phys.* **43** 144017

[11] van Rooij G J, Coenen J W, Aho-Mantila L, Brezinsek S, Clever M, Dux R, Groth M, Krieger K, Marsen S, Matthews G F, Meigs A, Neu R, Potzel S, Pütterich T, Rapp J, Stamp M F, the ASDEX Upgrade Team JET-EFDA Contributors 2013 *J. Nucl. Mater.* **438** S42

[12] Mao H, Ding F, Luo G N, Hu Z, Chen X, Xu F, Hu J, Zuo G, Sun Z, Yu Y, Wu J, Wang L, Duan Y, Xu J, Chen J, Yang Z, Ding R and Xie H 2017 *Nucl. Mater. Energy* **12** 447

[13] Duan Y M, Hu L Q, Mao S T, Xu P, Chen K Y, Lin S Y, Zhong G Q, Zhang J Z, Zhang L and Wang L 2011 *Plasma Sci. Technol.* **13** 546

[14] Xu J C, Wang L, Xu G S, Luo G N, Yao D M, Li Q, Cao L, Chen L, Zhang W, Liu S C, Wang H Q, Jia M N, Feng W, Deng G Z, Hu L Q, Wan B N, Li J, Sun Y W and Guo H Y 2016 *Rev. Sci. Instrum.* **87** 083504

[15] Zhang L, Morita S, Xu Z, Wu Z, Zhang P, Wu C, Gao W, Ohishi T, Goto M, Shen J, Chen Y, Liu X, Wang Y, Dong C, Zhang H, Huang X, Gong X, Hu L, Chen J, Zhang X, Wan B and Li J 2015 *Rev. Sci. Instrum.* **86** 123509

[16] Zhang L, Morita S, Xu Z, Zhang P F, Zang Q, Duan Y M, Liu H Q, Zhao H L, Ding F, Ohishi T, Gao W, Huang J, Yang X D, Chen Y J, Wu Z W, Xu P, Ding B J, Hu C D, Gong X Z, Chen J L and Hu L Q 2017 *Nucl. Mater. Energy* **12** 774

[17] Xu G S, Yuan Q P, Li K D, Wang L, Xu J C, Yang Q Q, Duan Y M, Meng L Y, Yang Z S, Ding F, Liu J B, Guo H Y, Wang H Q, Eldon D, Tao Y Q, Wu K, Yan N, Ding R, Wang Y F, Ye Y, Zhang L, Zhang T, Zang Q, Li Y Y, Liu H Q, Jia G Z, Liu X J, Si H, Li E Z, Zeng L, Qian J P, Lin S Y, Xu L Q, Wang H H, Gong X Z and Wan B N 2020 *Nucl. Fusion* **60** 086001

[18] Eckstein W 2002 *IPP-rep.*

[19] Ou J, Xiang N, Men Z Z, Zhang L, Xu J C and Gao W 2019 *Chin. Phys. B* **28** 125201

[20] Xu G, Zhou Y, Mao S, Kong D, Li L, Chan V and Ye M 2018 *IEEE Trans. Plasma Sci.* **46** 1382

[21] Xu Y, Xu G, Mao S and Ye M 2021 *Plasma Phys. Control. Fusion* **63** 095003

[22] Stangeby P C and Moulton D 2020 *Nucl. Fusion* **60** 106005

[23] Xiang H M, Zhang T, Wen F, Qu H, Wu M F, Geng K N, Li G S, Wang Y M, Han X, Liu Z X, Zhong F B, Ye K X, Zhang S B and Gao X 2018 *Rev. Sci. Instrum.* **89** 10H103

[24] Zhang Y P, Mazon D, Zou X L, Zhong W L, Gao J M, Zhang K, Sun P, Dong C F, Cui Z Y, Liu Y, Shi Z B, Yu D L, Cheng J, Jiang M, Xu J Q, Isobe M, Xiao G L, Chen W, Song S D, Bai X Y, Zhang P F, Yuan G L, Ji X Q, Li Y G, Zhou Y, Delpech L, Ekedahl A, Giruzzi G, Hoang T, Peysson Y, Song X M, Song X Y, Li X, Ding X T, Dong J Q, Yang Q W, Xu M, Duan X R and Liu Y 2018 *Nucl. Fusion* **58** 046018

[25] Zhang S, Gao X, Ling B, Wang Y, Zhang T, Han X, Liu Z, Bu J and Li J 2014 *Plasma Sci. Technol.* **16** 311